PAPER

Magnetically-assembled multifunctional magnetic-plasmonic SERS substrate for low-concentration analyte detection

To cite this article: Shilpa R Amonkar and Sudhir Cherukulappurath 2023 *Nanotechnology* **34** 445602

IOP Publishing Nanotechnology
Nanotechnology 34 (2023) 445602 (12pp) https://doi.org/10.1088/1361-6528/aceafc

Magnetically-assembled multifunctional magnetic-plasmonic SERS substrate for low-concentration analyte detection

Shilpa R Amonkar and Sudhir Cherukulappurath*

School of Physical and Applied Sciences, Goa University, Taleigao Plateau, Goa 403206, India

E-mail: sudhir.c@unigoa.ac.in

Received 1 June 2023, revised 22 July 2023
Accepted for publication 27 July 2023
Published 16 August 2023

Abstract

Multifunctional particles with combined magnetic and optical properties are promising materials for applications such as sensing and detection of analytes, and contrast agents for imaging techniques such as MRI, and photocatalysis. While the magnetic property allows for non-contact manipulation of the nanoparticles, optical properties can be harnessed for such sensing applications. We present the synthesis and large-scale assembly of inter-layered magnetic-plasmonic nanoparticles with graphene oxide (GO) spacer (Fe_3O_4@GO@Ag). The multifunctional composite particles were prepared using simple chemical methods and had an average size of 225 nm. The prepared samples were characterized using different techniques including powder XRD, FT-IR, Raman scattering, SEM, and TEM imaging. By using an external magnetic field, it is possible to form an assembly of these multifunctional particles on a large scale. Due to the chain-like formation in the presence of a magnetic field, such assemblies are good substrates for surface-enhanced Raman scattering (SERS). Here, we demonstrate the application of these magnetically-assembled particles for the detection of very low concentrations of analyte molecules (4-mercaptopyridine) using SERS. These multifunctional composite particles are good candidates for potential applications involving chemical detection, photocatalytic reactions, optoelectronic devices, and photothermal effects.

Supplementary material for this article is available online

Keywords: multifunctional nanoparticles, magnetic assembly, plasmonics, SERS

(Some figures may appear in colour only in the online journal)

Introduction

Multifunctional nanoparticles have been at the forefront of nanomaterial research in the recent decade owing to their potential in multifarious applications including biosensing, photocatalysis, photothermal processes, and detection of analytes [1–4]. It is desirous to have several properties such as magnetic, plasmonic, and luminescence combined into a single structure for such applications. In particular, there has been considerable effort to incorporate plasmonic metals into magnetic nanoparticles [5–17]. While plasmonic nanoparticles themselves have been proven useful in several applications such as biosensing and optoelectronics, the addition of magnetic properties can help in improving the efficiency of the process as well as for better manipulation. Several different configurations of plasmonic-magnetic nanostructures have been synthesized previously. With the emergence of graphene-based 2D materials, there have been attempts to study composites of magnetic-plasmonic nanoparticles and graphene-like structures [18–21]. The presence of graphene or graphene oxide not only allows for easy integration and adsorption of plasmonic nanoparticles but has also been reported to offer additional functionalities such as chemical enhancement of Raman scattering [22, 23]. By further incorporating plasmonic metals on such magnetic Fe_3O_4-graphene oxide (GO) nanoparticles, it opens up the

* Author to whom any correspondence should be addressed.

possibility of using these nanocomposites for enhanced-spectroscopic applications such as surface-enhanced Raman scattering (SERS) [22–26].

Self-assembly of nanoparticles provides a unique platform for several applications including bio-medical imaging, nanofabrication, chemical and biological sensing as well as the synthesis of supra-molecular materials [27, 28]. It involves either the directed or non-directed organization of individual particles into super-structures due to thermodynamic processes that can minimize the free energy. While natural self-assembly processes make use of weak forces such as van der Waals, electrostatic, or hydrodynamic, directed self-assembly can be beneficial for a more controlled, rapid, and large-scale synthesis of substrates [29]. In fact, such directed self-assembly of colloidal particles has fundamental importance and can have potential applications in spectroscopic measurements and transport mechanisms [30–40]. For instance, inkjet printing techniques based on electrohydrodynamics for the assembly of colloidal and plasmonic nanoparticles have been efficiently utilized for SERS applications [41]. Thermophoretic and dielectrophoretic forces have also been harnessed to aid the large-scale assembly of colloidal particles [42, 43]. For several applications, rapid assembly and disassembly are preferred and hence additional forces such as magnetic, optical, or thermophoretic can be utilized to speed up the otherwise slow diffusion-based self-assembly. While optical and thermophoretic assembly of colloidal particles, especially silica and plasmonic metal nanoparticles, are widely popular, the use of magnetic fields for large-scale assembly allows additional non-contact forces at a much larger scale [44–46]. It is known that magnetic self-assembly is a type of process in which a disordered system can organize itself due to local interactions among the magnetic particles that are influenced by an external magnetic field. Such long-range ordering occurs when molecules interact with one another through a balance of attractive and repulsive interactions in the presence of external magnetic fields [47]. The long-range assembly of magnetic nanoparticles is a complex process involving the coupling of dipole moments of each particle to the applied field, magnetic dipole–dipole interactions, the binding energy between the particles, and the surrounding environment. Magnetically assisted self-assembly of nanoparticles finds applications in energy storage and catalysis, [48, 49] preparation of 3D superstructures, [42–45] drug delivery, [50] and magnetic storage [51]. In fact, the presence of a magnetic core in multifunctional composite particles facilitates a large-scale manipulation of the structures with the help of external magnetic fields. The incorporation of plasmonic metals such as Ag or Au into such magnetic particles can be promising for surface-enhanced spectroscopic applications [22, 52, 53].

In this work, we use external magnetic fields to manipulate and assemble multifunctional Fe_3O_4@GO@Ag composite particles onto substrates. The multifunctional complexes were synthesized using chemical methods reported previously [54, 55]. The prepared samples were characterized using SEM, TEM, powder XRD, FT-IR, and Raman scattering. Large-scale assembly was performed using an external (bar or ring) magnet or an electromagnetic coil setup. The GO spacer layer between the magnetic Fe_3O_4 core and satellite Ag particles not only formed support but also helped in improving Raman signals by way of chemical enhancements [56–61]. This large-scale assembly was used as a SERS substrate for the detection of low concentrations of analyte molecule 4-mercaptopyridine (4-MPY).

Experimental methods

Synthesis of Fe_3O_4

The core Fe_3O_4 particles were synthesized using the hydrothermal method as described in the literature [62]. In brief, 2.77 g of $FeCl_3.6H_2O$ was added to 80 ml of ethylene glycol. To that, sodium acetate (7.22 g) was mixed, followed by the addition of 2 g of polyethylene glycol. The entire mixture was kept for stirring for an hour. Then, the mixture was transferred to a Teflon-lined autoclave and kept at 200 °C for 8 h in an oven. The resultant precipitate was removed and washed with ethanol several times after separating the particles using a bar magnet and kept for drying at 80 °C for 6 h.

Synthesis of Fe_3O_4@GO

GO was synthesized using a modified Hummer method [63]. In order to coat the Fe_3O_4 particles with GO, 0.1 g of the prepared Fe_3O_4 was dispersed in a mixture of 80 ml ethanol, 20 ml water, and 1 ml of ammonia solution followed by ultrasonication for half an hour. After this, 0.1 ml of tetraethyl orthosilicate (TEOS) and 0.1 ml of 3-aminopropyl triethoxysilane (APTMS) were added to the mixture and kept stirring for three hours. This was done to functionalize the Fe_3O_4 particles with an amine group. After three hours of stirring, the particles were separated from the solution and washed with an ethanol-water mixture several times to remove any residual solvents. 10 mg of GO powder (prepared by modified Hummer's method) was mixed with this amino-functionalized Fe_3O_4 in 10 ml water. This mixture was kept for sonication and then for vigorous stirring at 80 °C for 1 h. The obtained Fe_3O_4@GO particles were washed several times with deionized water.

Synthesis of Fe_3O_4@GO@Ag

In order to decorate the Fe_3O_4@GO composites with Ag nanoparticles, 0.17 g of $AgNO_3$ (0.1 M) was dissolved in 10 ml of water, 0.59 g of trisodium citrate was dissolved in 20 ml of water, and 0.16 g of NaOH (0.1 M concentration) was dissolved in 40 ml of water. Then, 2.5 ml of this freshly prepared $AgNO_3$ was dissolved in a solution of Fe_3O_4@GO (prepared as per the above procedure). After 30 min of stirring, 10 ml of aqueous solution of the prepared 0.1 M trisodium citrate, and 0.1 ml of NaOH were added. This entire mixture was kept for stirring for 6 h at 50 °C. The particle precipitate was then separated with an external magnet and washed with deionized water several times, and kept for drying in an oven for 2 h at 60 °C.

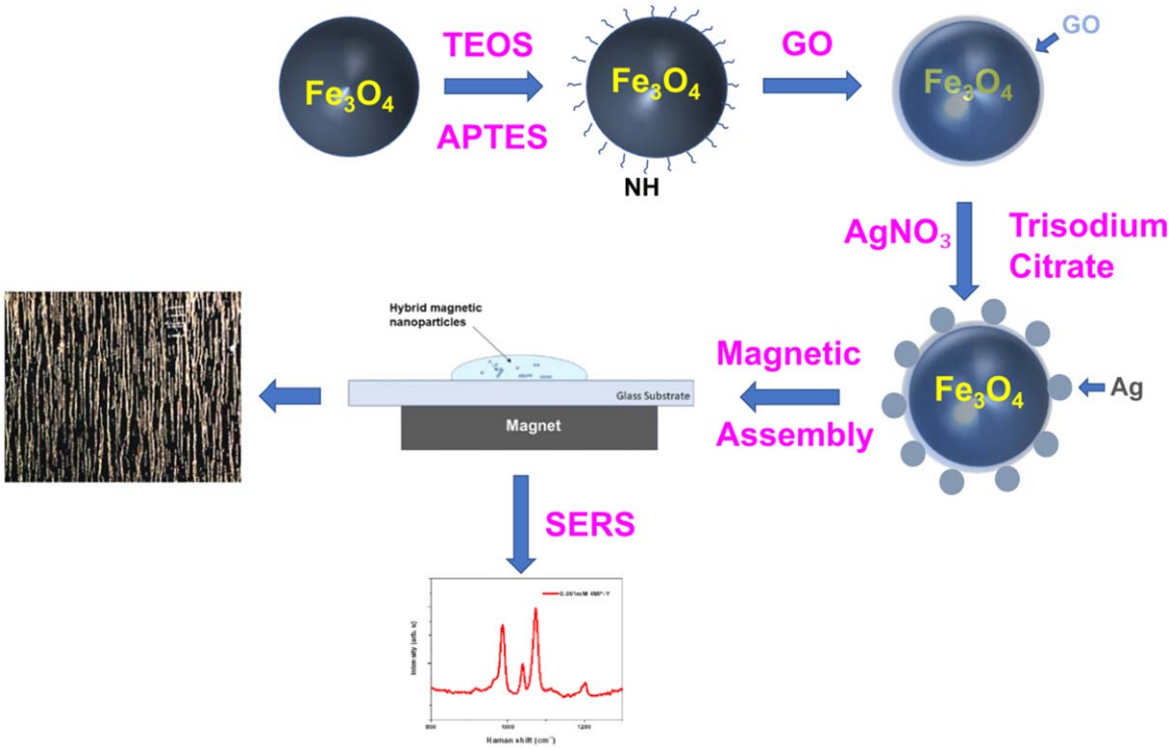

Figure 1. Schematic of the synthesis of magnetic-plasmonic nanocomposites and their alignment using the external magnetic field for SERS.

Materials characterization

Powder XRD pattern was obtained in the angle range of 10° −70°, using Cu-K_α radiation (1.5406 Å) with an operation voltage and current maintained at 40 kV and 50 mA. HR-TEM, selected-area electron diffraction (SAED), HAADF and EDAX images were taken on a 200 kV, Field-emission gun (FEG), TALOS F200S G2 TEM. Raman spectra and SERS of the samples were obtained using the LabRAM HR Evolution Raman system with a 532 nm laser source. Magnetic measurements were done using Lakeshore VSM 7410S.

Results and discussion

Characterization of Fe_3O_4@GO@Ag samples

In figure 1, a schematic of the synthesis process is shown. The details of synthesis have been described in the previous section. FTIR spectra of the samples are plotted in figure 2(a). The vibrational absorption of Fe_3O_4 corresponding to the stretching of Fe–O that is observed at 582 cm^{-1} is absent in Fe_3O_4@GO@Ag. The observed absorption at 1068 cm^{-1} indicates the successful formation of silica on Fe_3O_4. The peaks at 1387 cm^{-1} and 1628 cm^{-1}, confirm the presence of GO on the Fe_3O_4 particles. The transmission dip located at 1585 cm^{-1} is attributed to the remains of citrate on Ag nanoparticles surface [26, 50].

Powder XRD patterns of the prepared samples are shown in figure 2(b). The diffraction peaks for Fe_3O_4 structures showed an inverse spinel structure without any impurity peaks. The main peaks for Fe_3O_4 were found at 30.3°, 35.5°, 43.2°, 52.1°, 57.1°, 62.7° and 66.3° corresponding to the reflection planes of (220), (311), (400), (422), (511), (440), and (531) for the cubic spinel ferrite structure. The addition of GO on the Fe_3O_4 structures did not alter the diffraction peaks. No additional diffraction peaks were observable implying that the crystal structure remained unaffected in the process. After the incorporation of Ag particles on the Fe_3O_4@GO structures, the diffraction pattern showed additional peaks at 2θ values of 38.3°, 44.3°, 64.4° and 77.4° corresponding to Ag [22, 64]. This is also evident from the observation that increasing the concentration of Ag increased the intensity of the Ag diffraction peak. The crystallite size from Scherrer's equation of XRD analysis is found to be 24.3 ± 0.1 nm while the lattice parameter was estimated to be 8.39 ± 0.01 Å.

From the SEM image of the core Fe_3O_4 particles, the particles are spherical in shape and have an average size of 225 nm. The corresponding SEM image of Fe_3O_4@GO@Ag is given in supporting information figure S1. In order to confirm the presence of GO on the synthesized Fe_3O_4@GO particles, we performed Raman scattering experiments using a 532 nm laser. The powder sample was placed on a silicon substrate to reduce the autofluorescence signal from the glass at the wavelength. A typical Raman spectrum of the sample is shown in figure 2(d). The peaks at 190 cm^{-1}, 310 cm^{-1}, 520 cm^{-1}, and 660 cm^{-1} correspond to the ferrite vibrational modes ($3T_{2g}$ and A_{1g}) of Fe_3O_4 in accordance with the group theory of spinel structures [65–67]. The Raman peaks at 1361 cm^{-1} and 1593 cm^{-1} are attributed to the D and G bands of GO, respectively [18, 19].

In order to understand the morphology of the composite structures, TEM imaging of the sample was carried out.

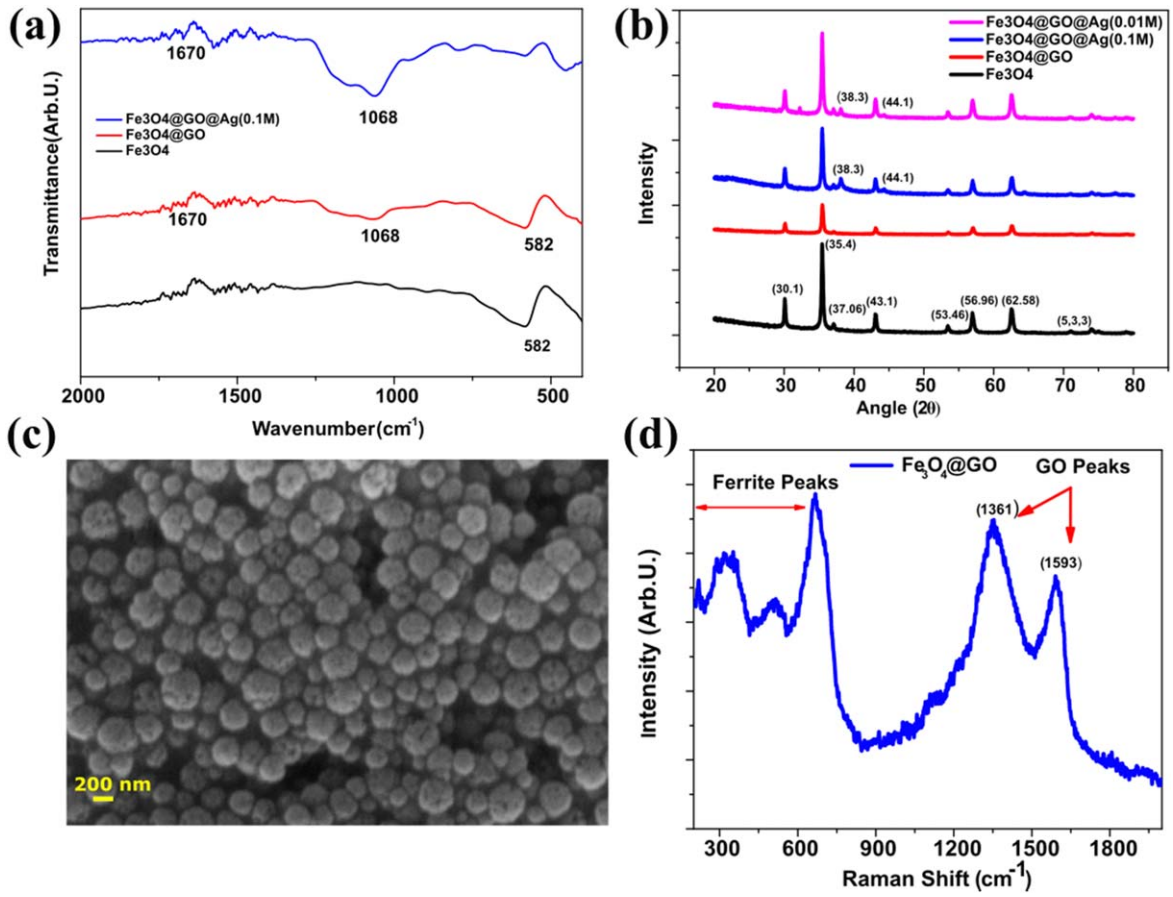

Figure 2. Characterization of the multifunctional structures (a) FT-IR spectra of the synthesized particles (b) Powder XRD spectra (c) SEM image of Fe_3O_4 core structure. The average particle size was estimated to be 225 nm. (d) Raman spectra of Fe_3O_4@GO reveal the ferrite Raman peaks below 800 cm^{-1} as well as the D and G peaks of GO at 1361 cm^{-1} and 1593 cm^{-1} respectively.

HR-TEM images along with electron diffraction patterns not only reveal the morphology and size of the magnetic particles but also the atomic arrangement. It was observed that the core Fe_3O_4 particles were monodisperse and nearly spherical in shape (figure 3(a)). A zoomed image of the particle is shown in figure 3(b). High-angle annular dark-field (HAADF) TEM image of the structure confirmed the presence of Fe (figure 3(c)). The corresponding images for Fe_3O_4@GO@Ag are shown in figures 3(d)–(f). The presence of a thin GO layer decorated with Ag nanoparticles can be observed from the TEM images. HR-TEM images (figures 3(g)–(i)) and SAED pattern (supplementary figure S2) of the nanostructures revealed the crystal planes of Fe_3O_4 and GO/Ag. SAED pattern showed several diffraction rings corresponding to the different planes of the crystal (figure S2). In the case of the Fe_3O_4 core, the lattice spacing for the (311) plane was estimated to be 0.25 nm (figure 3(h)) while that for the cubic Ag was found to be 0.24 nm. The major advantage of having magnetic nanoparticles in the composite structure is the presence of magnetic moments which can be utilized to manipulate the structures using an external magnetic field. However, the addition of other materials over the core magnetic particle can reduce the overall magnetic moment of the complex. In order to study the influence of additional materials (GO and Ag) on the magnetic properties of Fe_3O_4, we performed room-temperature magnetic measurements using a vibrating sample magnetometer. In figure 4, the magnetization curves for the synthesized samples are shown. It is observed that as the silver concentration in the nanocomposite is increased, the saturation magnetization of the overall composite decreases. It should be noted that although the magnetic moment of core Fe_3O_4 does not change by adding GO and Ag nanoparticles, there is a shielding of the magnetic field from the magnetic core of the composite thereby reducing the saturation magnetization of the composite particle compared to bare Fe_3O_4 particle. However, it is still possible to separate the particles from the solution using a magnet for a silver concentration of 0.1 M.

The saturation magnetization values for different samples are listed in table 1 below:

Magnetic field-aided self-assembly for SERS

In order to perform magnetic assembly of the particles, the solution containing Fe_3O_4@GO@Ag (2 mg ml^{-1}) was sonicated for 30 min to get monodispersed particles. An aliquot of 100 μl was drop-casted onto a pre-cleaned glass slide. The sample was placed on a magnet or between two bar magnets and allowed to dry overnight. The magnetically-assembled sample was observed using an upright microscope in both

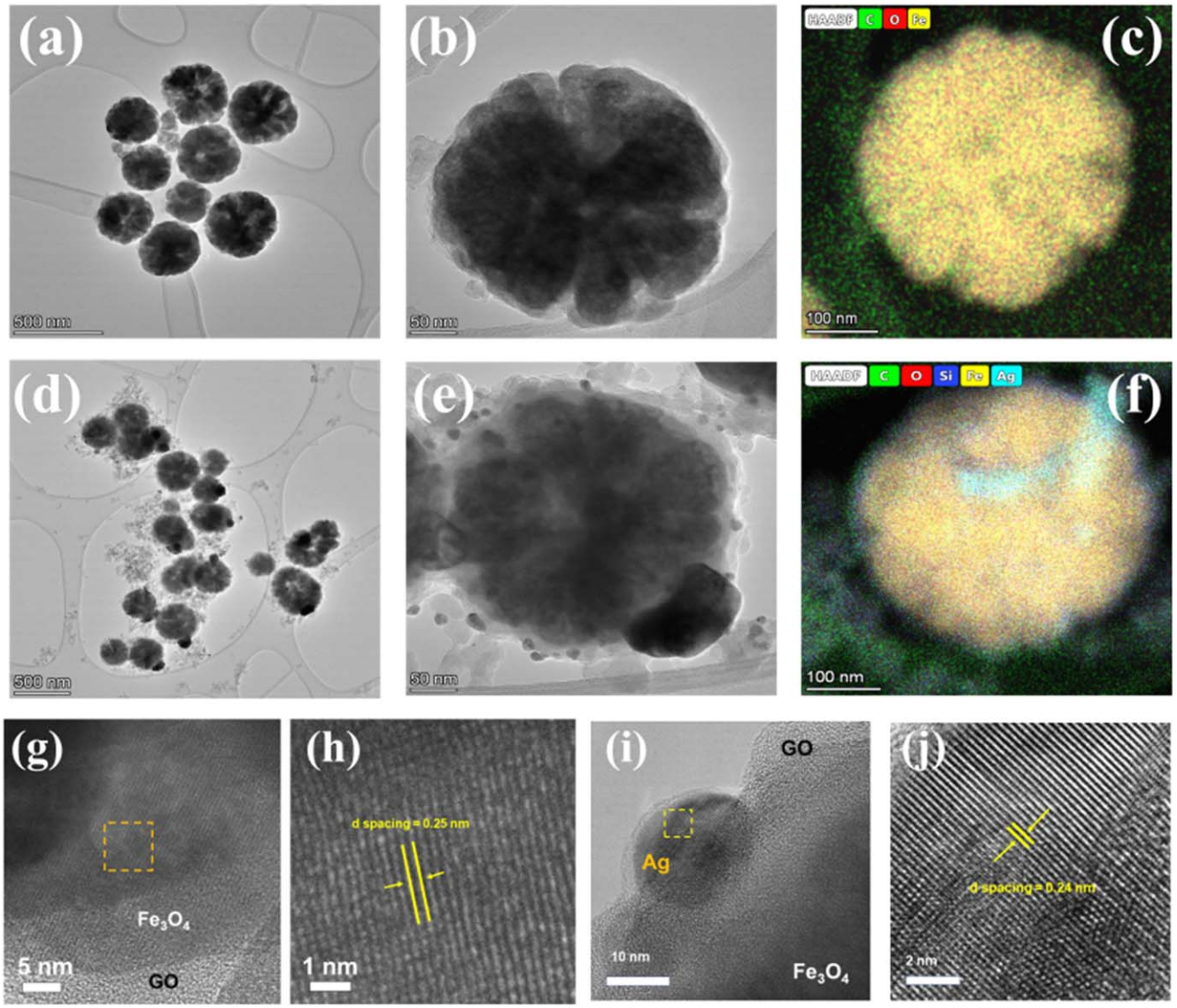

Figure 3. TEM images of the composites. (a) Fe_3O_4@GO particles. (b) Zoomed-in image of a single particle. (c) HAADF-TEM image of Fe_3O_4@GO shows the presence of Fe, O, and C. (d)–(f) Corresponding images for Fe_3O_4@GO@Ag. (g) HR-TEM image of Fe_3O_4@GO@Ag composite structure. (h) The zoomed image of (g) to estimate the lattice spacing for the (311) plane of Fe_3O_4. (i) and (j) correspond to Fe_3O_4@GO@Ag.

Table 1. Saturation magnetization values for different concentrations of Ag.

Sample	Saturation Magnetization (emu g^{-1})
Fe_3O_4	107.00
Fe_3O_4@GO	66.10
Fe_3O_4@GO@Ag (0.01 M)	60.23
Fe_3O_4@GO@Ag (0.1 M)	29.94

brightfield as well as dark field. In figure 5(a), a typical optical bright field image of the chain-like formation of the composite particles under the influence of the magnetic field can be observed. A zoomed image (figure 5(b)) reveals the formation of large-area chain-like structures due to the magnetic assembly. The nature of the assembly depends on the magnitude and direction of field strength. We used different configurations of the magnets in order to optimize the chain-like assembly. The samples placed directly on different positions of a ring magnet yielded different geometrical arrangements of the assembly. Placing the sample between two bar magnets with their attractive poles facing each other resulted in long chains compared to the other geometries. As the liquid dries under a magnetic field, the particles assemble towards the liquid boundary forming chain-like structures. The drying process itself can lead to self-assembly of colloidal particles. However, without any external magnetic field, the assembly process was very random. As expected, it is observed that the particles align in the direction of the strongest magnetic gradient. Hence depending on the position of the sample on the magnet, different directions of alignment are possible. In figures 5(c) and (d), the samples were placed in two different regions of the same magnet. It can be seen

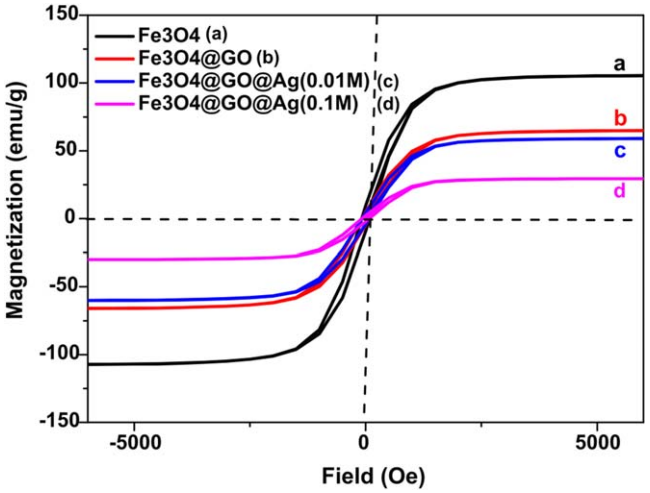

Figure 4. Magnetic measurements (*M–H*) for the multifunctional particles with varying amounts of Ag. The saturation magnetization of the composite particle was found to decrease with increasing Ag concentrations.

that the chains follow the direction of the magnetic field of the magnet (a ring magnet in this case), SEM images of such chains of magnetic nanoparticles is shown in supplementary information (figure S3). These images were taken after assembling the nanoparticles on a silicon substrate and drying the sample. It was observed that the micro-chain formation of the magnetic particles in a magnetic field was a rapid process. To visualize this in real-time, video was recorded using the CMOS camera attached to the microscope while the assembly occurs. Here the solution containing the magnetic nanoparticles was drop-casted onto a glass slide and placed under a microscope. An Nd bar magnet was placed in the vicinity of the sample to visualize the chain formation. In figure 5(e), the scenario without any magnetic field is shown. Initially, where there is no external magnetic field, the nanoparticles are randomly moving around in the solution by Brownian motion and diffusion. Within a few seconds of placing the magnet, the tiny particles start forming chains by attaching to each other. With time, a greater number of particles attach to the existing chains and form chain-like structures (figure 5 (fd)). The chains also move in the solution towards the direction of the magnet due to the effect of the magnetic force. Once the magnet is moved away from the sample, the movement is stopped and the assembly is collapsed. The video of the chain formation event is given in the supplementary data. The long chains of nanoparticles in the solution can easily be manipulated using the external magnet. It is possible to rotate the nanoparticle chains in all three directions using the bar magnet (see supplementary data). Interesting patterns can be observed in the optical images during the rotation of the chains. It was possible to attain three-dimensional manipulation of the magnetic chains in solution simply by moving the position of the magnet around the sample. It was also noted that under the influence of a magnetic field, these chains were stiff as if they were a single magnetic rod. Once the external magnetic field is removed, the particles remain attached (due to other weak forces) but lose the rod-like nature and collapse in the solution.

In order to obtain a uniform magnetic field, a bipolar electromagnet was used for the magnetic assembly instead of a bar/ring magnet. In this case, the magnetic field intensity could be controlled by varying the current through the coil. The solution was drop-casted onto a clean glass slide that was placed at the center of a bipolar electromagnet (see supplementary information figure S4 for a schematic of the experimental setup). A fixed current was passed through the coil and the sample was observed until the liquid evaporated. The optical dark-field images of assembled magnetic particles for different currents in the electromagnetic coil are shown in figures 6(a)–(d). It was observed that for no current through the coil, there was no structured assembly and the particles agglomerated randomly. For a current of 0.5 A (corresponding to a magnetic field of about 450 G at the center), the chain formation was noted (figure 6(a)). The assembly was thin and short in the case of low magnetic fields. With 1 A current in the coil (magnetic field of 840 G), the particles tend to form thicker as well as longer chains on the substrate (figures 6(b)–(c)). By increasing the current further to 2 A (magnetic field: 1640 G), the chain assembly was found to widen and overlap each other (see figure 6(d)). It should be noted that for all these different currents, the concentration of particles and volume of liquid was kept constant. From these observations, it is clear that a controlled large-scale assembly of magnetic-plasmonic nanoparticles can be achieved easily using the uniform magnetic field of the electromagnetic coil setup. These observations can open several possibilities for *in situ* manipulation of magnetic particles. In particular, large chains of hybrid magnetic-plasmonic structures can act as a good SERS substrate.

By incorporating noble metals such as Ag and Au, it is possible to use the chain-like features for the formation of electromagnetic hotspots that can enhance Raman signals several orders of magnitude. The presence of GO in the structures aided in facile functionalization. Apart from the electromagnetic enhancement of Raman signals due to the plasmonic excitations of Ag, it has been reported previously that by charge transfer effect of GO can improve the Raman signals by way of chemical enhancement [56, 57]. In order to test the capability of this scheme for SERS applications, we functionalized the substrates (chains of Fe_3O_4@GO@Ag) with different concentrations of 4-MPY. It is known that 4-MPY can easily attach to noble metals such as Au and Ag by means of the amine group present in the pyrimidine ring. In order to use the large-scale assembly of plasmonic-magnetic structures for SERS, we drop-casted different concentrations of 4-MPY on the substrate (magnetic-plasmonic nanoparticles on silicon). The solution was kept overnight and then mildly washed with DI water to remove unattached analyte molecules. The Raman spectra were obtained using a 532 nm laser anda 20x objective. The laser power was kept to 5 mW and the integration time was 10 s. The SERS spectra for 1 mM, 100 μM. 1 μM and 100 nm 4-MPY functionalized substrates are shown in figures 7(a)–(d) respectively. The salient peaks of 4-MPY at 790 cm^{-1} ascribed to the in-plane γ (CH) bond vibration, 1008 cm^{-1} to the ring breathing mode,

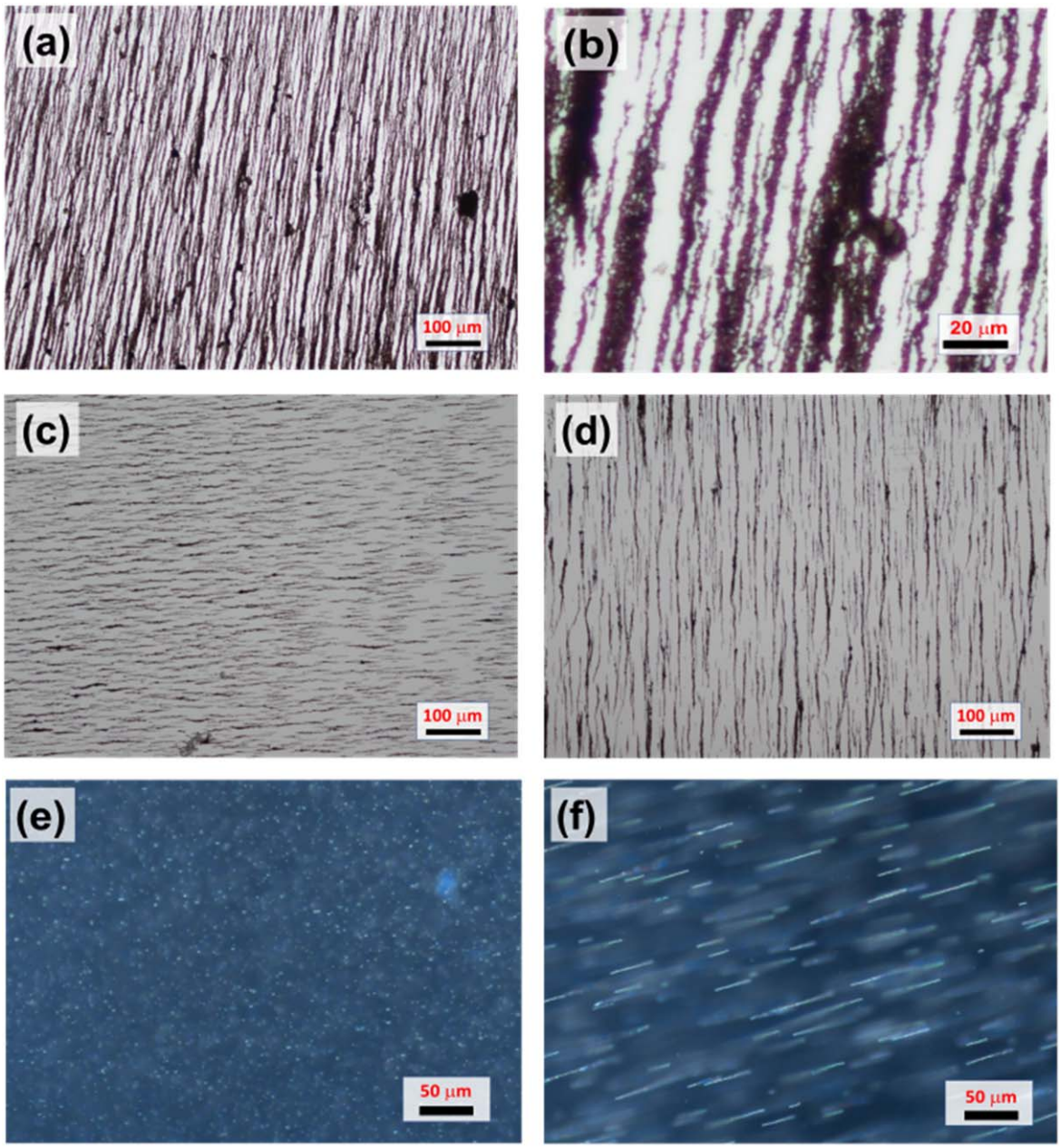

Figure 5. Magnetic self-assembly: the particles were suspended in an aqueous solution (1 mg ml^{-1} concentration) and placed over an Nd magnet and left for drying. (a) Optical image of the large-scale chain-like assembly of the composite structures obtained using a 10x objective. (b) Zoomed image of (a) shows a chain-like structure formed by magnetic materials under the influence of a magnet. (c) Optical image of chain formation of particles when the field lines are horizontal. (d) Chain formation in the vertical direction (e) optical phase-contrast image of the magnetic particles in solution. The particles can be seen as white dots. (f) After a few minutes of keeping the sample under the influence of a magnet, chain-like structures can be observed to be formed. The chain structures are rigid and can be rotated easily by rotating the magnetic field. Once the magnetic field is removed, the chains collapse in the solution although they still are held together loosely by van der Waal's forces. The video is available in supplementary data).

1040 cm^{-1} to the β(CH) mode, 1096 cm^{-1} to ring breathing mode, and ν(CS) mode and 1606 cm^{-1} to the ν(CC) vibrational modes can be observed in the 1 mM SERS signal (figure 7(a)) [68–71].

While random agglomeration of plasmonic nanoparticles (for example, due to the coffee-ring effect) has shown to give enhancement of Raman signals, [72, 73] a more controlled assembly is desirable for uniformity as well as higher enhancements [42, 74]. In order to check the uniformity of the substrate, SERS signals from 10 random positions on the sample were taken with similar conditions. It was observed that there was only a maximum of 10% variation between the SERS signals (figure S5 in supplementary information). From the comparison of intensities of Raman peaks at 1096 cm^{-1} for the SERS and 1 M neat solution, the enhancement factor was calculated to be 1.3×10^6. This value is an under-estimation as the number of molecules contributing to SERS is much lower on the SERS substrate.

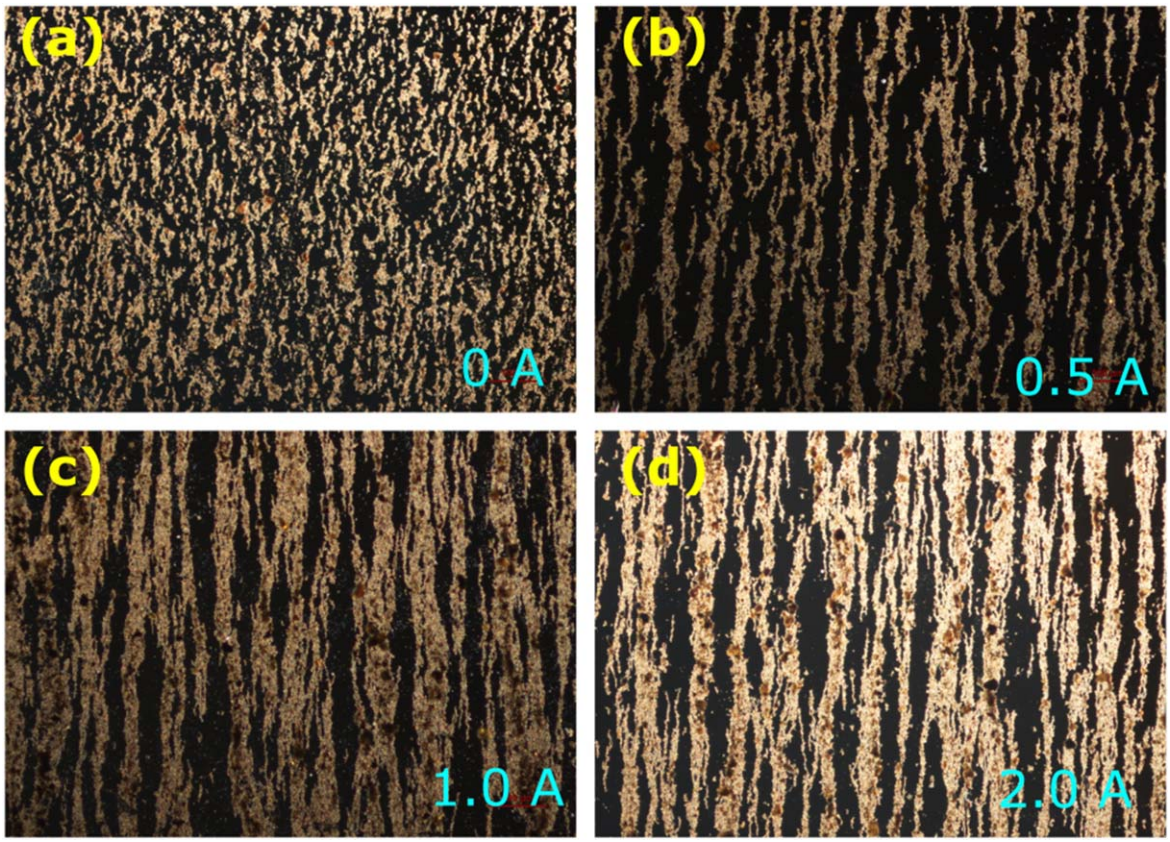

Figure 6. Large-scale magnetic assembly using electromagnetic coils. Darkfield optical image of the assembly of the multifunctional composite structures for various currents passed through the electromagnets. (a) 0 A (b) 0.5 A (450 G) (c) 1.0 A (840 G) (d) 2.0 A (1640 G).

In the case of very low concentrations of 4-MPY, although the intensity of the peaks was smaller, the molecule could be easily identified from the characteristic SERS spectra of 4-MPY. The two prominent peaks at 1096 cm^{-1} and 1008 cm^{-1} were clearly recognizable. For further lower concentrations of 4-MPY, 10 nm, and 1 nm, it was possible to observe the 1096 cm^{-1} peak in the SERS spectrum (figures 7(e) and (f)). However, for such low concentrations, the GO Raman peaks became significant. As the ratio of Fe_3O_4 to Ag was optimized for magnetic assembly, detection of the analyte with a further lower concentration required longer acquisition times or larger laser intensities. We believe that it is possible to detect concentrations below nM by increasing Ag to Fe_3O_4 ratio.

4-MPY has a C_{2v} symmetry and hence possess two in-plane (A_1, B_2) and two out-of-plane (A_2, B_1) vibrational modes which are Raman active. The out-of-plane vibrational modes are generally weak in aromatic ring compounds and therefore not predominant in the Raman spectrum of 4-MPY molecules [75, 76]. In SERS, the coupling of the aromatic ring with the plasmonic metal can occur in different ways. The relative enhancement factors can be different for different vibrational modes. In our SERS measurements, it was observed that the in-plane vibrational mode at 1095 cm^{-1} was most prominent and was detected even for the lowest concentration. The relative intensities of other peaks diminished drastically with decreasing concentration. The graphene oxide Raman spectra dominate the spectra in the wavelength region after 1300 cm^{-1} at low concentrations of 4-MPY. The main aim of the work was to use magnetically aided self-assembled particles as SERS substrates for the detection of analyte molecules. Further investigations need to be carried out to understand the nature of the spectrum at ultra-low concentrations in the single molecule regime.

Conclusion

In summary, multifunctional magnetic-plasmonic composites Fe_3O_4@GO@Ag were synthesized using chemical methods, and magnetic-field assisted large-scale assembly of these structures were demonstrated. Large-scale assembly of the multifunctional composites into chain-like structures was possible with the help of external magnetic fields. Each individual particle behaves as a tiny magnet under the influence of the external magnetic field thereby attracting other similar particles. Furthermore, the torque generated on the particles by the external magnetic field aligns the magnetic moment of the nanomagnets along the magnetic field. As the magnetic field is applied over a large area, the particles in the solution can form long chains on the substrate. Additionally, due to the presence of GO and Ag, such large-scale assemblies can be utilized as SERS substrates for analyte detection. Here the detection of 4-MPY at low concentrations using the magnetically

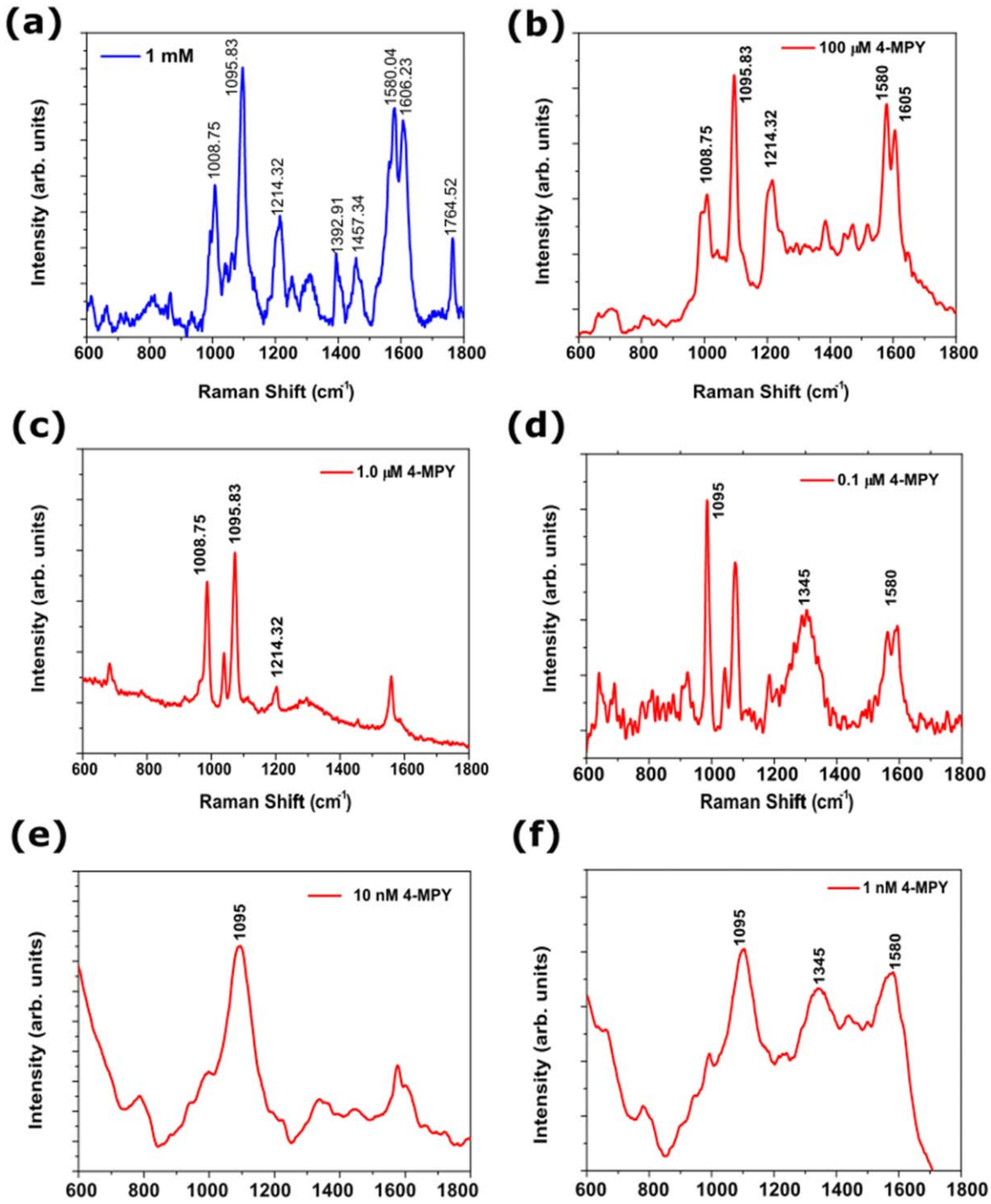

Figure 7. SERS Spectra of 4-MPY for different concentrations: SERS spectra was obtained by drop-casting the analyte molecules on the self-assembled structures. (a) 1 mM (b) 100 μM (c) 1 μM (d) 100 nm (e) 10 nm (f) 1 nm. The prominent vibrational peak at 1096 cm^{-1} is visible even at lower concentrations. At lower concentrations of the analyte molecules, the GO peaks become significant.

assembled particles was demonstrated. Due to their robustness and stability, these multifunctional particles can have potential applications for *in situ* sensing of analyte molecules wherein it is possible to manipulate them in a non-contact way with external magnetic fields. It is envisaged that these hybrid multifunctional structures will be promising candidates for the detection of environmental pollutants, catalysis, and photothermal applications.

Acknowledgments

The authors thank University Materials Characterization Laboratory (UMCL) at Goa University for the XRD and Raman measurements. SAIF IIT-Madras is acknowledged for VSM measurements. The authors would like to thank Dr Pralay K Santra for the HR-TEM images taken at the Centre for Nano and Soft Matter Sciences (CeNS), Bengaluru.

Data availability statement

All data that support the findings of this study are included within the article (and any supplementary files).

Supporting information, information is available online

SEM image of Fe_3O_4@GO@Ag and chain formation, TEM-SAED image, electromagnetic coil experimental setup, substrate uniformity test and enhancement factor calculation, videos of chain formation and external manipulation.

Notes

The authors declare no competing financial interests.

ORCID iDs

Sudhir Cherukulappurath https://orcid.org/0000-0003-1875-8066

References

[1] Lee D-E, Koo H, Sun I-C, Ryu J H, Kim K and Kwon I C 2012 Multifunctional nanoparticles for multimodal imaging and theragnosis *Chem. Soc. Rev.* **41** 2656–72
[2] Seleci M, Ag Seleci D, Joncyzk R, Stahl F, Blume C and Scheper T 2016 Smart multifunctional nanoparticles in nanomedicine *BioNanoMaterials* **17** 33–41
[3] Thomas S, Kalarikkal N and Abraham A R (ed) 2021 *Fundamentals and Properties of Multifunctional Nanomaterials* (Elsevier) (https://doi.org/10.1016/C2019-0-00953-3)
[4] Thomas S, Kalarikkal N and Abraham A R (ed) 2023 *Applications of Multifunctional Nanomaterials* (Elsevier) (elsevier.com/books/applications-of-multifunctional-nanomaterials/thomas)
[5] Shevchenko E V, Bodnarchuk M I, Kovalenko M V, Talapin D V, Smith R K, Aloni S, Heiss W and Alivisatos A P 2008 Gold/Iron oxide core/hollow-shell nanoparticles *Adv. Mater.* **20** 4323–9
[6] Levin C S, Hofmann C, Ali T A, Kelly A T, Morosan E, Nordlander P, Whitmire K H and Halas N J 2009 Magnetic−plasmonic core-shell nanoparticles *ACS Nano* **3** 1379–88
[7] Niehues M, Engel S and Ravoo B J 2021 Photo-responsive self-assembly of plasmonic magnetic Janus nanoparticles *Langmuir* **37** 11123–30
[8] Zeng J, Gong M, Wang D, Li M, Xu W, Li Z, Li S, Zhang D, Yan Z and Yin Y 2019 Direct synthesis of water-dispersible magnetic/plasmonic heteronanostructures for multimodality biomedical imaging *Nano Lett.* **19** 3011–8
[9] Huang L, Ao L, Hu D, Wang W, Sheng Z and Su W 2016 Magneto-plasmonic nanocapsules for multimodal-imaging and magnetically guided combination cancer therapy *Chem. Mater.* **28** 5896–904
[10] Yu H, Chen M, Rice P M, Wang S X, White R L and Sun S 2005 Dumbbell-like bifunctional Au−Fe_3O_4 nanoparticles *Nano Lett.* **5** 379–82
[11] Peng S, Lei C, Ren Y, Cook R E and Sun Y 2011 Plasmonic/magnetic bifunctional nanoparticles *Angew. Chemie Int. Ed.* **50** 3158–63
[12] Hui W, Shi F, Yan K, Peng M, Cheng X, Luo Y, Chen X, Roy V A L, Cui Y and Wang Z 2012 Fe_3O_4/Au/Fe_3O_4 nanoflowers exhibiting tunable saturation magnetization and enhanced bioconjugation *Nanoscale* **4** 747–51
[13] Mao Y, Yi P, Deng Z and Ge J 2013 Fe_3O_4–Ag heterostructure nanocrystals with tunable Ag domains and magnetic properties *CrystEngComm* **15** 3575–81
[14] Sharma V K, Siskova K M and Zboril R 2013 Magnetic bimetallic Fe/Ag nanoparticles: decontamination and antimicrobial agents. in interactions of nanomaterials with emerging environmental contaminants *ACS Symp. Ser.* **1150** 11–193 American Chemical Society
[15] Ha M, Kim J-H, You M, Li Q, Fan C and Nam J-M 2019 Multicomponent plasmonic nanoparticles: from heterostructured nanoparticles to colloidal composite nanostructures *Chem. Rev.* **119** 12208–78
[16] Amendola V *et al* 2014 Magneto-plasmonic Au–Fe alloy nanoparticles designed for multimodal SERS-MRI-CT imaging *Small* **10** 2476–86
[17] León Félix L, Sanz B, Sebastián V, Torres T E, Sousa M H, Coaquira J A H, Ibarra M R and Goya G F 2019 Gold-decorated magnetic nanoparticles design for hyperthermia applications and as a potential platform for their surface-functionalization *Sci. Rep.* **9** 4185
[18] Peik-See T, Pandikumar A, Ngee L H, Ming H N and Hua C C 2014 Magnetically separable reduced graphene oxide/iron oxide nanocomposite materials for environmental remediation *Catal. Sci. Technol.* **4** 4396–405
[19] Kahsay M H, Belachew N, Tadesse A and Basavaiah K 2020 Magnetite nanoparticle decorated reduced graphene oxide for adsorptive removal of crystal violet and antifungal activities *RSC Adv.* **10** 34916–27
[20] Banerjee S, Benjwal P, Singh M and Kar K K 2018 Graphene oxide (RGO)-metal oxide (TiO_2/Fe_3O_4) based nanocomposites for the removal of methylene blue *Appl. Surf. Sci.* **439** 560–8
[21] Wang J F, Wu X Z, Wang C W, Shao N S, Dong P T, Xiao R and Wang S Q 2015 Magnetically assisted surface-enhanced Raman spectroscopy for the detection of staphylococcus aureus based on aptamer recognition *ACS Appl. Mater. Interfaces* **7** 20919
[22] Liu Z, Wang Y, Deng R, Yang L, Yu S, Xu S and Xu W 2016 Fe_3O_4@Graphene oxide@Ag particles for surface magnet solid-phase extraction surface-enhanced Raman scattering (SMSPE-SERS): from sample pretreatment to detection all-in-one *ACS Appl. Mater. Interfaces* **8** 14160–8
[23] Zhang C, Huang L, Pu H and Sun D-W 2021 Magnetic surface-enhanced Raman scattering (MagSERS) biosensors for microbial food safety: fundamentals and applications *Trends Food Sci. Technol.* **113** 366–81
[24] Huynh K-H *et al* 2021 Recent advances in surface-enhanced Raman scattering magnetic plasmonic particles for bioapplications *Nanomaterials* **11** 1215
[25] Xu J, Wang C, Rong Z, Cheng X and Xiao R 2015 A graphene-interlayered magnetic composite as a multifunctional SERS substrate *RSC Adv.* **5** 62101–9
[26] Kavyani S and Baharfar R 2020 Design and characterization of Fe_3O_4 /GO/Au–Ag nanocomposite as an efficient catalyst for the green synthesis of spirooxindole-dihydropyridines: Fe_3O_4/GO/Au-Ag catalyst for synthesis of spirooxindole *Appl. Organomet. Chem.* **34** e5560
[27] Whitesides G M, Kriebel J K and Mayers B T 2005 Self-assembly and nanostructured materials BT - nanoscale assembly: chemical techniques ed W T S Huck (Springer US) pp 217–39

[28] Li Z, Fan Q and Yin Y 2022 Colloidal self-assembly approaches to smart nanostructured materials *Chem. Rev.* **122** 4976–5067

[29] Grzelczak M, Vermant J, Furst E M and Liz-Marzán L M 2010 Directed self-assembly of nanoparticles *ACS Nano* **4** 3591–605

[30] Klokkenburg M, Vonk C, Claesson E M, Meeldijk J D, Erné B H and Philipse A P 2004 Direct imaging of zero-field dipolar structures in colloidal dispersions of synthetic magnetite *J. Am. Chem. Soc.* **126** 16706–7

[31] Sahoo Y, Cheon M, Wang S, Luo H, Furlani E P and Prasad P N 2004 Field-directed self-assembly of magnetic nanoparticles *J. Phys. Chem.* B **108** 3380–3

[32] Neugebauer N, Fabian A, Elm M T, Hofmann D M, Czerner M, Heiliger C and Klar P J 2020 Investigation of the dipole interaction in and between ordered arrangements of magnetic nanoparticles *Phys. Rev.* B **101** 104409

[33] Cheng G, Romero D, Fraser G T and Hight Walker A R 2005 Magnetic-field-induced assemblies of cobalt nanoparticles *Langmuir* **21** 12055–9

[34] Alphandéry E, Ding Y, Ngo A T, Wang Z L, Wu L F and Pileni M P 2009 Assemblies of aligned magnetotactic bacteria and extracted magnetosomes: what is the main factor responsible for the magnetic anisotropy? *ACS Nano* **3** 1539–47

[35] Zhang Y, Sun L, Fu Y, Huang Z C, Bai X J, Zhai Y, Du J and Zhai H R 2009 The shape anisotropy in the magnetic field-assisted self-assembly chain-like structure of magnetite *J. Phys. Chem.* C **113** 8152–7

[36] Li L, Yang Y, Ding J and Xue J 2010 Synthesis of magnetite nanooctahedra and their magnetic field-induced two-/three-dimensional superstructure *Chem. Mater.* **22** 3183–91

[37] Tracy J B and Crawford T M 2013 Magnetic field-directed self-assembly of magnetic nanoparticles *MRS Bull.* **38** 915–20

[38] Velez C, Torres-Díaz I, Maldonado-Camargo L, Rinaldi C and Arnold D P 2015 Magnetic assembly and cross-linking of nanoparticles for releasable magnetic microstructures *ACS Nano* **9** 10165–72

[39] Crawford T M 2017 *9.14—self-assembled magnetic materials* (Elsevier) pp 257–72 Atwood, J. L. B. T.-C. S. C. I. I.

[40] Das S and Dutta A 2018 Field-assisted growth of magnetic nanoparticle supercrystals *Mater. Res. Express* **5** 106104

[41] Pekdemir S, Torun I, Sakir M, Ruzi M, Rogers J A and Onses M S 2020 Chemical funneling of colloidal gold nanoparticles on printed arrays of end-grafted polymers for plasmonic applications *ACS Nano* **14** 8276–86

[42] Cherukulappurath S, Lee S H, Campos A, Haynes C L and Oh S-H 2014 Rapid and sensitive in situ SERS detection using dielectrophoresis *Chem. Mater.* **26** 2445–2452

[43] Joby J P, Das S, Pinapati P, Rogez B, Baffou G, Tiwari D K and Cherukulappurath S 2022 Optically-assisted thermophoretic reversible assembly of colloidal particles and e. coli using graphene oxide microstructures *Sci. Rep.* **12** 3657

[44] Shetye S B, Agashe J S and Arnold D P 2007 Investigation of microscale magnetic forces for magnet array self-assembly *IEEE Trans. Magn.* **43** 2713–5

[45] Hangarter C M, Rheem Y, Yoo B, Yang E-H and Myung N V 2007 Hierarchical magnetic assembly of nanowires *Nanotechnology* **18** 205305

[46] Mehdizadeh Taheri S *et al* 2015 Self-assembly of smallest magnetic particles *Proc. Natl Acad. Sci.* **112** 14484–9

[47] Lim J, Lanni C, Evarts E R, Lanni F, Tilton R D and Majetich S A 2011 Magnetophoresis of nanoparticles *ACS Nano* **5** 217–26

[48] Wang X, Wang T, Borovilas J, He X, Du S and Yang Y 2019 Vertically-aligned nanostructures for electrochemical energy storage *Nano Res.* **12** 2002–17

[49] Ekeroth S, Münger E P, Boyd R, Ekspong J, Wågberg T, Edman L, Brenning N and Helmersson U 2018 Catalytic nano truss structures realized by magnetic self-assembly in pulsed plasma *Nano Lett.* **18** 3132–7

[50] Helseth L E, Fischer T M and Johansen T H 2004 Magnetic structuring and transport of colloids at interfaces *J. Magn. Magn. Mater.* **277** 245–50

[51] Henderson J, Shi S, Cakmaktepe S and Crawford T M 2012 Pattern transfer nanomanufacturing using magnetic recording for programmed nanoparticle assembly *Nanotechnology* **23** 185304

[52] Tang X H, Dong R L, Yang L B and Liu J H 2015 Fabrication of Au nanorod-coated Fe_3O_4 microspheres as SERS substrate for pesticide analysis by near-infrared excitation *J. Raman Spectrosc.* **46** 470

[53] Gong T, Huang Y, Wei Z, Huang W, Wei X and Zhang X 2020 Magnetic assembled 3D SERS substrate for sensitive detection of pesticide residue in soil *Nanotechnology* **31** 205501

[54] Liang K J, Li X Q, Kang S Z, Qin L X, Li G D and Mu J 2014 Catalytic performance of ferroferric oxide/reduced graphene oxide/silver nanoparticle composite microflowers *Carbon* **80** 716 N. Y.

[55] Kavyani S and Baharfar R 2020 Design and characterization of Fe_3O_4/GO/Au–Ag nanocomposite as an efficient catalyst for the green synthesis of spirooxindole-dihydropyridines *Appl. Organomet. Chem.* **34** e5560

[56] Ling X, Xie L, Fang Y, Xu H, Zhang H, Kong J, Dresselhaus M S, Zhang J and Liu Z 2010 Can graphene Be used as a substrate for Raman enhancement? *Nano Lett.* **10** 553–61

[57] Ling X, Moura L G, Pimenta M A and Zhang J 2012 Charge-transfer mechanism in graphene-enhanced raman scattering *J. Phys. Chem.* C **116** 25112–8

[58] Yu X, Cai H, Zhang W, Li X, Pan N, Luo Y, Wang X and Hou J G 2011 Tuning chemical enhancement of SERS by controlling the chemical reduction of graphene oxide nanosheets *ACS Nano* **5** 952–8

[59] Kwon Y-B, Cho S Y, Jang H, Kim J-H and Kim Y-K 2021 Lateral size effect of graphene oxide on its surface-enhanced Raman scattering property *Langmuir* **37** 14205–13

[60] Lin J, Zhang N, Tong L and Zhang J 2016 Enhanced Raman scattering on graphene and beyond. in frontiers of plasmon-enhanced spectroscopy volume 2 *ACS Symp. Ser.* **1246** 5–97 American Chemical Society

[61] Zhang L, Bao Z, Yu X, Dai P, Zhu J, Wu M, Li G, Liu X, Sun Z and Chen C 2016 Rational design of α-Fe2O3/ reduced graphene oxide composites: rapid detection and effective removal of organic pollutants *ACS Appl. Mater. Interfaces* **8** 6431–8

[62] Deng H, Li X, Peng Q, Wang X, Chen J and Li Y 2005 Monodisperse magnetic single-crystal ferrite microspheres. *Angew. Chemie Int. Ed.* **44** 2782–5

[63] Marcano D C, Kosynkin D V, Berlin J M, Sinitskii A, Sun Z, Slesarev A, Alemany L B, Lu W and Tour J M 2010 Improved synthesis of graphene oxide *ACS Nano* **4** 4806–14

[64] Xia H, Cui B, Zhou J, Zhang L, Zhang J, Guo X and Guo H 2011 Synthesis and characterization of Fe_3O_4@C@Ag nanocomposites and their antibacterial performance *Appl. Surf. Sci.* **257** 9397–402

[65] de Faria D L A, Venâncio Silva S and de Oliveira M T 1997 Raman microspectroscopy of some iron oxides and oxyhydroxides *J. Raman Spectrosc.* **28** 873–8

[66] Testa-Anta M, Ramos-Docampo M A, Comesaña-Hermo M, Rivas-Murias B and Salgueiriño V 2019 Raman spectroscopy to unravel the magnetic properties of iron oxide nanocrystals for bio-related applications *Nanoscale Adv.* **1** 2086–103

[67] Soler M A G and Qu F 2012 Raman spectroscopy of iron oxide nanoparticles BT *Raman Spectroscopy for Nanomaterials Characterization* ed C S S R Kumar (Springer) pp 379–416
[68] Muniz-Miranda M, Neto N and Sbrana G 1988 Surface-enhanced raman spectra of pyrazine, pyrimidine, and pyridazine adsorbed on silver sols *J. Phys. Chem.* **92** 954–9
[69] Baldwin J A, Vlčková B, Andrews M P and Butler I S 1997 Surface-enhanced Raman scattering of mercaptopyridines and pyrazinamide incorporated in silver colloid−adsorbate films *Langmuir* **13** 3744–51
[70] Cardini G, Muniz-Miranda M and Schettino V 2004 SERS and DFT Study on 4-methylpyridine adsorbed on silver colloids and electrodes *J. Phys. Chem.* B **108** 17007–11
[71] Song W, Wang Y and Zhao B 2007 Surface-enhanced Raman scattering of 4-mercaptopyridine on the surface of TiO2 nanofibers coated with ag nanoparticles *J. Phys. Chem.* C **111** 12786–91
[72] Wang W, Yin Y, Tan Z and Liu J 2014 Coffee-ring effect-based simultaneous SERS substrate fabrication and analyte enrichment for trace analysis *Nanoscale* **6** 9588–93
[73] Šimáková P, Kočišová E and Procházka M 2021 'Coffee ring' effect of Ag colloidal nanoparticles dried on glass: impact to surface-enhanced Raman scattering (SERS) *J. Nanomater.* **2021** 4009352
[74] Cho H, Lee B, Liu G L, Agarwal A and Lee L P 2009 Label-free and highly sensitive biomolecular detection using SERS and electrokinetic preconcentration *Lab Chip* **9** 3360–3
[75] Hu J, Zhao B, Xu W, Li B and Fan Y 2002 Surface-enhanced Raman spectroscopy study on the structure changes of 4-mercaptopyridine adsorbed on silver substrates and silver colloids *Spectrochim. Acta* A **58** 2827–34
[76] Xu S, Tang W, Chase D B, Sparks D L and Rabolt J F 2018 A highly sensitive, selective, and reproducible SERS sensor for detection of trace metalloids in the environment *ACS Appl. Nano Mater.* **1** 1257–64